Boulder dislodgement during coastal storms and tsunamis: Insights from a new ensemble model

Robert Weiss[a,c], Jennifer Irish[b,c], Beverly Goodman Tchernov[d,e]

[a]*Department of Geosciences, Virginia Tech, VA 24061, U.S.A.*
[b]*Department of Civil and Environmental Engineering, Virginia Tech, VA 24061, U.S.A.*
[c]*Center for Coastal Studies, Virginia Tech, VA 24061, U.S.A.*
[d]*Department of Marine Geosciences, University of Haifa, Israel*
[e]*Morris Kahn Marine Station, Kibbutz Sdot Yam, University of Haifa, Israel*

Abstract

Boulders are excellent candidate deposits to study coastal inundation events by storms and tsunamis due to their significant preservation potential. However, it is difficult to infer how and what forcing dislodged the boulder. We present a new model that enables ensemble and Monte-Carlo-type simulations to study the sensitivity of boulder, the fluid flow, and environmental parameters. Our examples show that boulder transport is complex and nonlinear, and to acknowledge the uncertainties of the boulder's preexisting transport conditions, a range of velocities and environmental parameters should be used to quantify the flow that caused boulder dislodgement.

Keywords: Coastal Boulders, Tsunami, Storms, Monte Carlo Simulations

1. Introduction

1.1. General Context

Coastal boulders are important because they document extreme wave actions, such as those that occur during storms and tsunamis. Furthermore, boulders are a unique type of deposit as they can consist of only few "particles". Nott (2003) demonstrated that information about the pre-transport setting of boulders is important. A variety of different approaches have been developed to consider boulder motion, assuming different pre-transport settings and simplifying assumption about the hydrodynamic forcing to quantify the storm or tsunami that moved boulders. We refer to Cox et al. (2020) for more information about Nott's 2003 approach, the most common approach from which others, such as Benner et al. (2010),Nandasena et al. (2011b), Nandasena et al. (2011a), Buckley et al. (2012), and Barbano et al. (2010), are derived. More fundamentally, if information about the causative events is available, and better yet, data that can be used to calibrate hydrodynamic models, boulder transport can be understood at a much more advanced level (see for example, Watanabe et al., 2019, and references therein). However, very often, especially for historic events or events in the geologic record, such information is not available–including the pre-transport setting of the boulder. None of the existing approaches can accommodate the ambiguity related to the causative process and pre-transport setting in a consistent manner. To address this shortcoming, we present a Monte-Carlo-type ensemble model with the capability to sample parameter distributions that describe the uncertainties around the pre-transport setting as well as how the flow interacts with the boulder.

Boulders as heavy as 50 or 80 tonnes have been reported as moved by storms (Cox et al., 2012) and tsunamis (Dewey and Ryan, 2017). Just the fact that hydrodynamic forces during storms and tsunamis are capable of transporting such large particles is in itself astonishing and should narrate a cautionary tale independent of the causative process. However, much of the debate, when it comes to boulder deposits during coastal hazard events, is focused on whether the boulders were moved during a tsunami or a storm. Of course, it is important to delineate the causative boulder movement processes for hazard assessment, as while both storms and tsunamis can have devastating effects, they do vary in their coastal inundation, duration, and the character of how they impact the coastline. However, especially without enhanced knowledge and specific information about the hydrodynamic forcing, it remains difficult to defend a conclusion regarding whether a storm or a tsunami caused the motion of a boulder. Advanced numerical simulations, such as presented in Zainali and Weiss (2015), Kennedy et al. (2016) and Watanabe et al. (2019) are capable, but the wealth of information needed to create the input waves has only been recorded by tide gauges, wave buoys, or other measuring devices in the past few decades. Without these existing constraints, advanced simulations produce speculations rather than certainties about the conditions that lead to boulder transport. To emphasize this consideration, we have to acknowledge that waves in a tsunami or storm are best characterized by a wave

spectrum, which provides information about the presence of certain amplitudes and how often a certain amplitude occurs. However, it does not provide the true sequencing of the waves, and information on how these wave amplitudes interact with each other as they propagate. In this context, wave-wave interactions can create hydrodynamic forcing capable of moving boulders in an area some distance from where the spectrum measurement was taken (e.g., wave buoy); in other words, these interactions can create local amplitudes that are above the maximum amplitude component of the observed spectrum. The opposite on the lower end is also possible for boulders not having been moved (Weiss and Sheremet, 2017). Because of this fact, our model output is the relationship of boulder motion given flow depth and flow velocity for a given boulder mass, where we consider other parameters to be random and sample them from a distribution.

1.2. Geometric Setup and Study

Figure 1 depicts the boulder transport problem. We assume that a boulder's geometry can be simplified by a rectangular prism whose length is a, width is b and height is c. While a rectangular prism is still an idealized representation of the boulder, when compared to a sphere, a rectangular prism much more closely aligns with realistic boulder shapes seen in the field. Importantly, the rectangular prism allows us to consider boulder shapes with aspect ratios other than one, namely, boulders with one dimension measurably longer than another. Note that for simplicity, we define the wave arrival perpendicular to the length of the boulder. Additionally, note that this axis definition differs from the one classically used in boulder studies, in which a defines the longest boulder dimension while c denotes the shortest boulder dimension. Figure 1 also contains all the forces that directly contribute to boulder movement, along with their respective moment arms for overturning about the axes' origin. For more discussion on the forces, their moment arms, and how they relate to the equations of motion, we refer to section *2 Theoretical Background*. The general setting for the boulder is on a uniform slope of angle α, where the boulder has to overcome the roughness δ to move into a position that allows dislodgement (dotted rectangle in Fig. 1). The angle that the boulder rotation has to exceed to reach a position where it remains dislodged once the event is over–the critical position for permanent dislodgement –is referred to as the critical angle θ_c. In the case of a fully submerged homogeneous boulder, the physical definition for the critical angle is when the center of mass (black dots in Fig. 1) is directly above the pivot point (vertically aligned). For more information on the paradigm that is behind this assumption, we refer to Weiss and Diplas (2015) and references therein. The roughness can have any value from zero to the height of the boulder. For the case when the roughness δ is zero, boulder sliding is also possible. Nandasena et al. (2011b) and Nandasena et al. (2011a) also calculated conditions for rotation and sliding, showing the sliding scenario requires a lower velocity for motion. From a physical point of view, as long as the center of mass of the boulder is above the pivot point, the boulder can rotate towards the critical dislodgement position. If the center of mass of the boulder is below that point, rotation becomes impossible

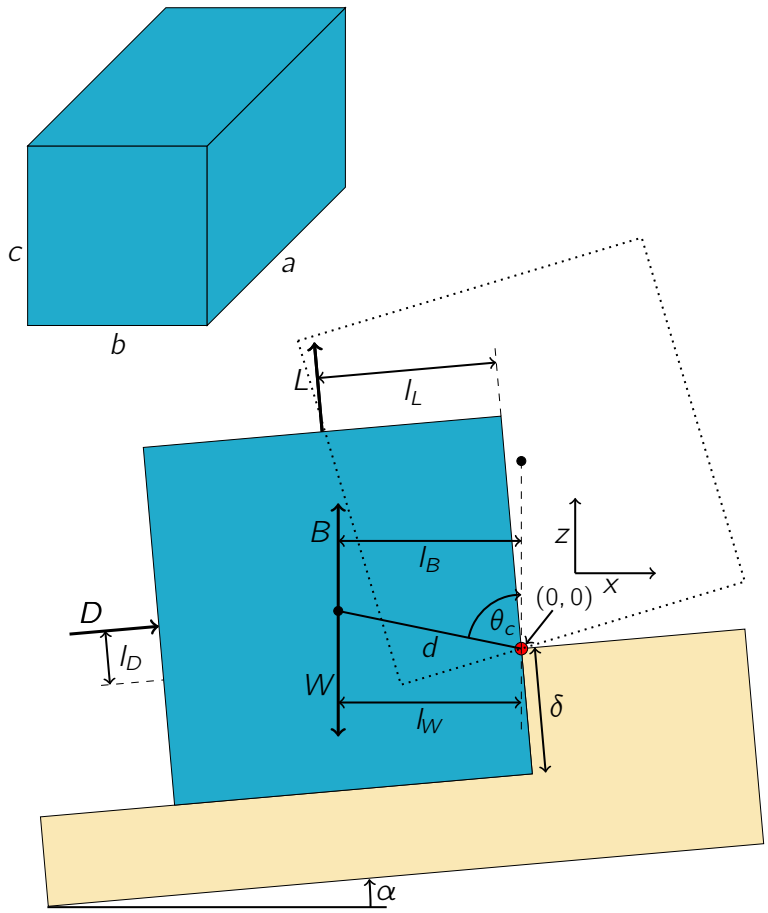

Figure 1: Geometric definition of the boulder-dislodgement problem including forces and lever arms. The dashed boulder indicates the position the boulder has to move to to dislodge.

because a positive moment cannot occur. Yet, it has been observed in the field that boulders were dislodged whose height is approximately equal to the roughness δ. For example, Switzer and Burston (2010) reported on boulders that were quarried from a rock unit located nearshore that exhibit the same thickness as the transported boulders. In this case and other situations where the vertical position of the center of the mass of the boulder is below the pivot point, in order for the boulder to overturn it must first be lifted, a process that we refer to as vertical sliding because the boulder moves upward. If the roughness δ is zero, it is also possible that the boulder slides along the slope, hereafter referred to as "along-slope sliding". We assume that along-slope sliding is an irreversible motion that does not allow for the boulder to return to its original position. Therefore, we define the motion of the boulder by length b as dislodged.

In our contribution, we generally follow the approach outlined by Weiss and Diplas (2015) and employ Newton's Second Law of Motion for the rotational motion toward the critical dislodgement position, depending on the height c of the boulder compared to the roughness δ this also includes vertical sliding. Furthermore, we consider along-slope sliding in the case of $\delta = 0$. We generally refer to a boulder to be dislodged if a

boulder's movement exceeds the critical angle of dislodgement in the rotational case or travels the length of b in case of along-slope sliding. As in Weiss and Diplas (2015), we calculate how the boulder moved from its original to a position from which onward dislodgement occurs. We assume that this is the minimum requirement for recognizable boulder movement in the field. How the boulder moved with the flow after the critical dislodgement position is exceeded is complex and will most likely be influenced by a complex interaction of multiple waves in both tsunamis and storms. Furthermore, the simplicity of the approach also generates uncertainties arising from the simplifications employed. Most notably, the coefficients and constants, mostly used for the calculation of forces, are difficult to constrain and are potentially a significant source of uncertainty in the results. Instead of trying to justify a specific coefficient or constant's magnitude, for example, for the drag and lift coefficients, we treat these coefficients and constants as random parameters that are sampled from a physically defensible interval given a uniform probability for each sample. This has the advantage that uncertainties coming, for example, from the data, such as the boulder dimensions and density, can be treated in the same fashion, resulting in a more statistically defensible result, which, by extension, also means a more physically defensible result.

2. Theoretical Background

Within a Monte-Carlo framework we investigate herein boulder dislodgement by rotation and sliding, or a combination of both, by assuming idealized flow conditions and that the boulder may be represented as a rectangular prism –with respect to spheres, a more realistic representation of boulder geometries occurring in nature (Fig. 1). Below, we introduce the form of the governing equations of motion used herein, namely, the conservation of angular momentum for rotation (following Weiss and Diplas, 2015) and conservation of linear momentum for sliding, then discuss characterization of the dynamic forces the fluid exerts on the boulder, the criteria for boulder dislodgement, and implementation within a Monte-Carlo framework.

2.1. Governing Equation for Rotation

If roughness is present in front of the boulder, the movement of the boulder toward dislodgement can be simplified by a rotational motion. Therefore, the predominant equation of motion is the conservation of angular momentum, written in terms of the moments exerted on the boulder and the mass moment of inertia:

$$I\frac{\mathrm{d}^2\theta}{\mathrm{d}t^2} = \sum M_a \tag{1}$$

in which I refers to the mass moment of inertia and M_a to the moments. In the presented geometry, the mass moment of inertia is governed by the relationship between b and c and whether the boulder is fully submerged or if it starts or becomes emergent during any part of its movement. Fig. 2 depicts the initial conditions and a later time during movement toward dislodgement for the fully submerged and partially submerged cases. For

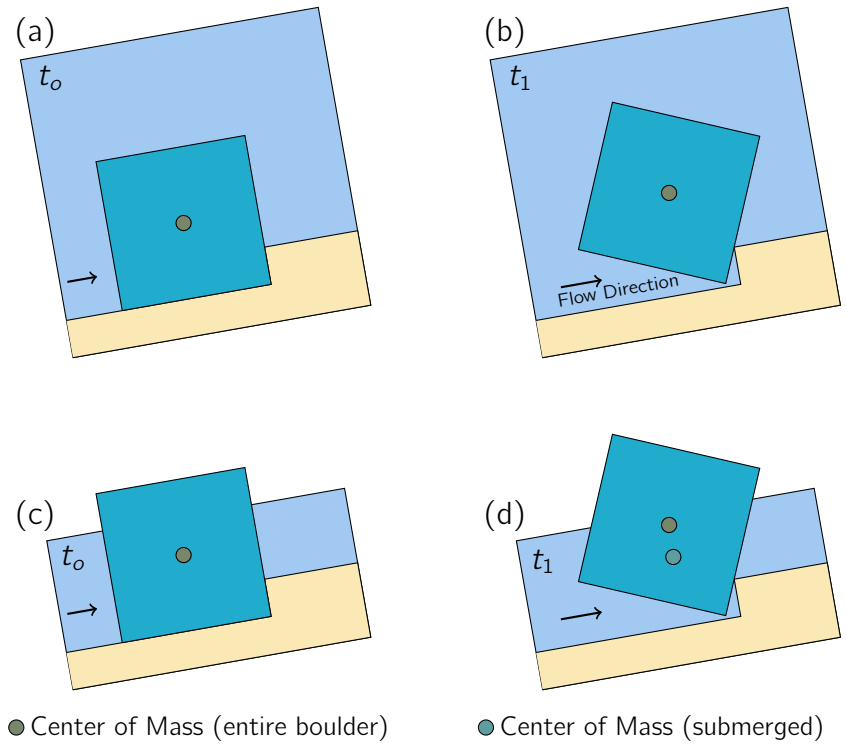

Figure 2: Fully submerged (a & b) and partially submerged (c & d) boulder dislodgement. For the partially submerged boulder, we see the distance between the Centers of Mass of the entire boulder and of the submerged portion changes with boulder position, i.e., between the original position (t_0, c) and later position (t_1, d), as the boulder moves toward the dislodgement position.

the governing equations, it is important to consider the fact that water is displaced as the boulder moves. For the fully submerged case, the volume of water that has to be displaced is proportional to some fraction of the entire boulder volume; while in the partially submerged case, the fraction of displaced water is proportional to the portion of the boulder that is in the water. The water that has to be displaced is referred to as added or virtual mass in the literature, such that the effective mass that is to be moved is the sum of the mass of the body plus a fraction of the equivalent water mass: $m = m_s + m_v$, where m_v is approximated by $C_m V_s \rho$ (V_s – volume of boulder, C_m – added mass coefficient, and ρ – water density). This added mass effect appears in the angular momentum balance via the mass moment of inertia in Eq. 1, yielding: $I = I_s + I_v$. To calculate I_s and I_v for the conditions presented in Fig. 1, we integrate the boulder mass along the horizontal and vertical axes of the boulder geometry to calculate the mass moment of inertia of both coordinates if the rotation would be respectively around the horizontal axis, I_x and the vertical axis I_z. The perpendicular axis theorem, $J_y = I_x + I_z$, then allows us to move the rotation axis to one along the boulder length a passing through the Center of Mass, of the entire boulder for I_s and of the submerged portion of the boulder for I_v. Finally, we

apply the parallel axes theorem, $J_y + md^2$, where d denotes the distance between the center of mass and the desired location, in this case the pivot point marked by the red dot in Fig. 1. Based on this method, we can derive the following equation for I_s and I_v for the fully submerged case (Fig 2a):

$$I_{s,v} = \frac{1}{12} m_{s,v}(b^2 + c^2) + m_{s,v}\left[\frac{4}{3}b^2 + \frac{1}{3}c^2 + \left(c - \frac{\delta}{2}\right)^2\right] \tag{2}$$

Substituting Eq. (2) for I_s and I_v, we then can rewrite Eq. (1) for the fully submerged case (Fig. 2a) to:

$$\frac{1}{4}V_s\left[\frac{1}{3}\left(b^2 + c^2\right) + \left(b^2 + [c - 2\delta]^2\right)\right](\rho_s + C_m\rho)\frac{\mathrm{d}^2\theta}{\mathrm{d}t^2} = \sum M_a \tag{3}$$

As mentioned, Eq. (3) can only be applied to fully submerged boulders. If, however, in the case where the boulder starts or becomes emergent due to a relatively small flow depth compared to the boulder's height, the shape of the submerged portion of the boulder is no longer of a rectangular cross section. In this case, we approximate I_x and I_z with

$$I_x = \rho a A_p \frac{1}{12}\sum_{i=1}^{n-1}\left(z_i^2 + z_i z_{i+1} + z_{i+1}^2\right)\left(x_i z_{i+1} - x_{i+1} z_i\right) \tag{4}$$

$$I_z = \rho a A_p \frac{1}{12}\sum_{i=1}^{n-1}\left(x_i^2 + x_i x_{i+1} + x_{i+1}^2\right)\left(x_i z_{i+1} - x_{i+1} z_i\right) \tag{5}$$

where x_i and z_i are the coordinates of the polygon defining the shape of the submerged portion of the boulder. To obtain I_v, we substitute Eqs. (4) and (5) into the perpendicular axis theorem mentioned earlier and apply the parallel axis theorem by adding md^2. Here the parameter d is the distance from the center of displaced fluid mass (c_x, c_z) and the pivot point, which for polygons is calculated with the help of the method proposed by Bourke (1988): $d^2 = c_x^2 + c_z^2$ because the pivot point is located at the origin (see 1). The mass m is calculated by $m = \rho a A_p$, where A_p is the area of the polygon describing the shape of the submerged portion of the boulder (in the x-z plane in 1) and is computed after Bourke (1988).

The sum of the moments on the right-hand side of Eq. (1) is analogous to the sum of the forces on the right-hand side of Newton's Second Law of Motion, or the conservation of linear momentum equation ($F = ma$). A moment is defined to be a force multiplied with its lever arm, defined as the perpendicular distance between the force vector and the axis of rotation. In our case, the forces that are important are the boulder weight W, buoyancy B, and the dynamic fluid forces–modeled here as drag force D and lift force L. For the general case, the weight of the boulder acts at the center of mass of the entire boulder, while the buoyancy acts at the center of mass of the submerged portion of the boulder. By this definition, the moment arm of the weight is the horizontal component of the center of mass of the entire boulder, while the moment arm of buoyancy is the horizontal component of the center of the submerged boulder mass (c_x). In cases where the boulder is fully submerged, these centers of mass are coincident. The actual distribution of

dynamic fluid force on a submerged body is complex, and we assume here the resultant dynamic fluid force is represented by a drag and a lift component (see section 2.3) such that the lever arms for the drag and lift forces are respectively measured perpendicular to and in line with the upstream flow direction. For simplicity, we assume the magnitude of these lever arms is equal to one-half of the projected wetted area into the flow for drag and parallel to the flow for lift.

As given in Eq. 1 and other aforementioned equations, the sum of the moments, $\sum M_a$, on the right-hand side is an important part of the equations of motion. In our case, the moments are, not surprisingly, related to drag ($l_D D$), lift ($l_l L$), Weight (l_W), and buoyancy ($l_B B$). For drag and lift, we employ the classical quadratic form (see below). For Figure 1 provides an overview of how drag, lift, weight, and buoyancy relate to each other and how the respective levers are determined. Based on these relationships, the sum of the moments yields: $\sum M_a = l_D D + l_L L + l_B B - l_W W$. Note that the sum moments is adjusted to accommodate the slope, α, and for the case of partially submerged boulders.

2.2. Governing Equations for Sliding

Sliding occurs in the proposed model in two ways: (a) sliding along the slope (x') if the roughness δ is zero (along-slope sliding), and (b) sliding perpendicular to the slope (z') (vertical sliding). Note that friction between the boulder and the slope will be considered, but describes a material behavior during the sliding process rather than a geometric characteristic of the setup; in other words, friction accounts for roughness elements that are too small to prevent sliding along the slope. Furthermore, we assume vertical sliding is a dominant process only when roughness δ is nonzero and the center of mass of the boulder is initially located below the pivot point of the dislodgement movement, where we neglect vertical sliding otherwise. The equations of motion for sliding are conservation of linear momentum along the slope and perpendicular to the slope:

$$m\frac{\mathrm{d}^2 x'}{\mathrm{d}t^2} = D - \mu_{x'}(W - B)\cos\alpha \tag{6}$$

$$m\frac{\mathrm{d}^2 z'}{\mathrm{d}t^2} = L - \mu_{z'}(W - B)\sin\alpha \tag{7}$$

where $\mu_{x'}$ and $\mu_{z'}$ are the friction coefficients. The last terms in each equation represent the friction forces exerted by the surrounding ground (Eq. 6) or the side of the roughness element with height δ (Eq. 7) on the boulder, and is proportional to the boulder's net weight, $W - B$. Including the added mass effect, because the boulder is fully or partially submerged, the full equations of motion are:

$$(m_s + C_m m_f)\frac{\mathrm{d}^2 x'}{\mathrm{d}t^2} = D - \mu_{x'}(W - B)\cos\alpha \tag{8}$$

$$(m_s + C_m m_f)\frac{\mathrm{d}^2 z'}{\mathrm{d}t^2} = L - \mu_{z'}(W - B)\sin\alpha \tag{9}$$

where m_f for the partially submerged case is again calculated after Bourke (1988). Equation 8 for along-slope sliding and Eq. 9 for vertical sliding are applied respectively with the $\mu_{x'}$ as a random parameter, and $\mu_{z'}$ equal to one for simplicity (maybe make this a variable).

2.3. Drag and Lift Forces

We employ the classical quadratic form of drag and lift forces, $\{D, L\} = \frac{1}{2}\rho C_{\{d,l\}} A_{\{d,l\}} u^2$ where $C_{\{d,l\}}$ denotes the drag and lift coefficients, $A_{\{d,l\}}$ is the characteristic area on which the drag or lift coefficient is based, ρ is the water density, and u is upstream flow speed. As innocent as the quadratic forms for drag and lift appear, there are significant complexities hidden in $A_{\{d,l\}}$, $C_{\{d,l\}}$ and even u.

Here, we take A_d as the boulder's projected wetted area into the flow and A_l as the projected wetted area in-line with the flow. With the given boulder-axes definition in Fig. 1 we can see that at rest for the fully submerged case, the area for the drag is $a \times c$ and for lift is $a \times b$. For the partially submerged case, however, the area for the drag is calculated by $a \times \eta$, where η denotes the water depth. When the boulder starts moving toward the dislodgement position, the boulder's characteristic areas for drag and lift may change. For example, in Fig. 2b, the height of the area for drag is now much bigger because the rotating boulder is diagonally positioned in the flow. However, in the partially submerged case, the area related to the drag force does not change because it is simply controlled by the water depth. In the same fashion, the area related to the lift force changes as well. It is worth noting that in the partially submerged case, the orientation of the boulder as well as the water depth are important when calculating the drag- and lift-related areas.

Another important factor for drag and lift is the respective coefficients $C_{\{d,l\}}$. Most commonly, both coefficients are determined for bodies at rest. Reported coefficients have been determined either with the help of experiments or numerical models, by analyzing the forces, their respective effective area, and the present flow velocity. Therefore, choosing the most accurate value for both lift and drag coefficients is very difficult if not impossible for any given water depth and boulder shape. To mitigate this apparent problem, we assume that the drag and lift coefficients are part of the uncertainty that boulder transport problems carry. This assumption enables us to employ both drag and lift coefficients as random variables (over given intervals) in a Monte-Carlo framework.

As mentioned earlier, most considerations of the quadratic lift and drag forces are for bodies at rest. However, in the problem of interest here the boulder is moving, either rotating toward the dislodgement position or sliding. Therefore, the fluid velocity u needs to be adjusted with the help of the respective boulder velocity. In the case of sliding, the adjustment is $u - \frac{\mathrm{d}x}{\mathrm{d}t}$. For rotation toward the dislodgement position, we assume that the velocity adjustment can be expressed by the component of the velocity at the boulder's center of mass that is in-line with the slope. The velocity in the quadratic drag and lift forces can thus be replaced by $u - \frac{\mathrm{d}x'}{\mathrm{d}t}|_G$, where subscript G marks the center of gravity.

2.4. Conditions for Boulder Dislodgement

In the case of rotation, the dotted rectangle in Fig. 1 illustrates the critical position for permanent dislodgement; namely the location when the static (no flow) moments sum to zero, $l_x + l_z = 0$, beyond which the boulder overturns when the dynamic fluid forcing is removed. Even when rotation occurs, if the sum of the moments in Eq. 3 become and remain smaller than zero before the boulder reaches this critical position, the boulder will move back to its original position (Weiss and Diplas, 2015) and will not dislodge.

For the fully submerged case, the moment levers for the weight and buoyancy are both located at the center of mass of the boulder, and when the boulder reaches the critical position for dislodgement, both moments arms become zero. However, the situation for the partially submerged case is different because the moment arm for the weight is related to the center of mass of the entire boulder (black circle in Fig. 2d), but for the buoyancy moment arm the reference point is the center of mass only of the submerged part (red circle in Fig. 2d). Both centers of mass can be situated at different vertical distances from the pivot axis of the boulder rotation.

While this condition is generally applicable to all rotation cases, for the fully submerged case, the critical angle, as depicted in Fig 1 is

$$\theta_c = \frac{\pi}{2} - \alpha - \arctan\left(\frac{c/2 - \delta}{b/2}\right) \tag{10}$$

While Eq. (10) is strictly valid only for a fully submerged boulder, we observed a negligible difference in predicting dislodgement when using the critical angle condition for the fully submerged case as the critical condition for the partially submerged case; specifically, differences between the actual and estimated criteria for partially submerged conditions only changed the timing of when the dislodgement occurred but did not change whether dislodgement occurred. Because of that fact, we argue the difference can be ignored, and we employ the critical angle in Eq. (10) in all our computations. If the boulder exceeds the critical angle of rotation, θ_c, and can no longer move back to its original position, we refer to this situation as *dislodgement by rotation*.

To define a dislodgement criterion for along-slope sliding is more complicated. For simplicity, we refer to the case where the boulder slid the distance equivalent to axis b or more during the interaction with the flow as *dislodgement by sliding*. In the situation where neither dislodgement by sliding nor rotation occurs, and to be complete, we simply refer to *no dislodgement*.

2.5. Other Random Parameters and Monte-Carlo Framework

As stated in section 2.3, the drag and lift coefficients are treated as random parameters sampled from given intervals. In the case of sliding, the friction coefficient is equally difficult to determine robustly. We, therefore, treat the friction coefficient as a random parameter following the same arguments as the drag and lift coefficients.

Another important parameter that carries significant uncertainty is the added or virtual mass coefficient C_m, especially comparing the fully submerged and partially submerged cases. For simple geometries, such as a sphere or cylinder, constants for C_m have been characterized and reported in every Fluid Mechanics textbook.However, rectangular cross-sections, especially in the presence of roughness, have not been well studied. There seems to be no standard method for estimating the actual value during the motion process. Therefore, we also treat the added mass coefficient C_m as a random parameter.

The remaining random parameters include boulder density ρ_s, flow depth η, and flow speed u. All parameters that are considered random parameters are sampled, in here, with uniform probability between given minimum and maximum values.

There are a total of seven random parameters considered herein in the Monte-Carlo framework. Instead of creating a seven-dimensional parameter space, we chose to randomize each random parameter for each realization. The dimensions of the boulder (axes a, b, and c) are important input parameters that, we assume are determined in the field with some level of accuracy or estimated with some level of confidence. It should be noted that setting up all or either of the boulder dimensions as a random parameter in the Monte Carlo framework can be accomplished with little programming effort.

3. Results

3.1. Time Series of Boulder Movement

Figure 3 depicts the motion of a boulder toward the critical conditions for dislodgement for slope angles of $\alpha = 0^o$ and $\alpha = 10^o$. For the 5 illustrative cases shown in this figure, the mass is constant. The initial positions are depicted as solid rectangles; while the dislodgement positions are indicated by a dotted rectangle. A simple rotation without roughness δ is shown in Fig. 3a (case I refers to $\alpha = 0^o$ and case II to $\alpha = 10^o$). Both curves end when the critical angle is reached. Comparing cases I and II, we can see how the critical angle increases as the slope increases, but also the profound effect the slope has on the time needed for the boulder to reach the critical position for dislodgement. In this example, the critical position for dislodgement is reached after $t(\theta = \theta_c) \equiv t_c = 1s$ for case I and $t_c = 2.4s$ for case II.

Figure 3b shows the impact of roughness. Case I is the same as in Fig. 3a. Case III is likewise for a slope angle of $\alpha = 0^o$, but additionally includes roughness that exceeds the vertical position of the center of mass. As mentioned earlier, it is physically impossible for the boulder to rotate toward the dislodgement position from its initial position in this case because a positive moment for the drag, for example, cannot be achieved. For a boulder to be dislodged from this position, the boulder has to slide vertically until a positive moment is possible, which at a minimum occurs when the vertical position of the center of mass is in line with the pivot point. In this case, we can also easily see that for $\alpha = 0^o$ (dashed rectangle), the critical angle is

$\theta_c = \frac{\pi}{2}$. The vertical sliding takes time and increases the time when the boulder reaches the critical position for dislodgement to $t_c = 4.0s$.

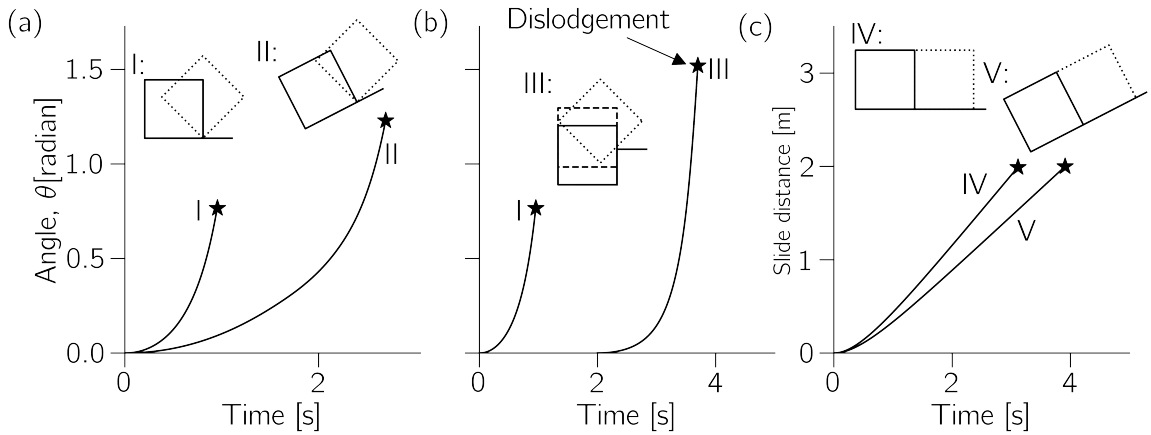

Figure 3: Time series of different dislodgement scenarios up to the point when the critical position for dislodgement is reached: (a) rotation for slope angles of $\alpha = 0^o$ (I) and $\alpha = 15^o$ (II) (higher hydrodynamic forcing than in dislodgement by sliding case), (b) rotation with vertical sliding when roughness $\delta > 0.5c$ (the highest hydrodynamic forcing needed for dislodgement), and (c) along-slope sliding for slope angles of $\alpha = 0^o$ (I) and $\alpha = 15^o$ (II) (the lowest hydrodynamic forcing resulting in dislodgement). The curve marked with I in (b) refers to the case I in (a), indicating rotation on a horizontal plane for comparison.

Figure 3c shows sliding as the dislodgement mode for the case when $\delta = 0$. The critical distance that the boulder has to slide is set to half of the boulder width. Case IV refers to the horizontal slope case ($\alpha = 0$); while the slope for case V is $\alpha = 10^o$. We can see that the impact of the slope on when the critical position is reached is not as dramatic as it is for cases I and II.

3.2. Dislodgement by Sliding and Rotation

A boulder can dislodge either by rotation or sliding. Dislodgement by sliding is only possible if the roughness δ is zero, while rotation is possible for all roughness values. Figure 4 depicts example results with varying slopes and roughness values. For these numerical experiments, the boulder density is kept constant at $\rho = 1800kg\,m^{-3}$, and the boulder dimensions are $2m \times 2m \times 2m$. The flow depth ranges from $1m$ to $20m$, and the flow speed ranges from $0.5ms^{-1}$ to $15ms^{-1}$.

For Fig. 4a, both roughness and slope are zero, which enables dislodgement by sliding alone (green) and by both rotation and sliding (orange). For dislodgement by sliding, the flow speed varies between $3.1ms^{-1}$ for the lower boundary to the no-dislodgement cases (in blue) and $4.7ms^{-1}$ for the transition to the area in the $u - \eta$ phase space where both dislodgement by both rotation and sliding can occur for flow depths larger than $2.0m$, which coincides with the height c of the boulder. For flow depths smaller than $2.00m$, the dislodgement flow speed increases linearly from $3.1ms^{-1}$ for $\eta = 2.0$ to $7.9ms^{-1}$ for $\eta = 1.00m$ for the transition from no

dislodgement to dislodgement by sliding; while the transition from dislodgement by sliding only (green) and dislodgement by both rotation and sliding (orange) increases from $4.7ms^{-1}$ at $\eta = 2.00m$ to $u = 10.7ms^{-1}$ at $\eta = 1.00m$. The roughness is zero and the slope is 10° for Fig. 4b. The transition of constant to linearly increasing flow speeds takes place at $\eta = 2.0m$ for dislodgement by along-slope sliding and rotation (green). Dislodgement by sliding occurs between $3.5ms^{-1}$ and $5.0ms^{-1}$ in the constant part, and increases to the same values as in Fig. 4a (lower part $7.9ms^{-1}$, upper part $10.7ms^{-1}$). Dislodgement by rotation takes place for flow speeds exceeding the upper boundary of the dislodgement by sliding interval.

In Fig. 4c, where the roughness is 0.8 m and the slope is zero, the transition to a constant flow speed for increasing flow depth also takes place at $\eta = 2.00m$. The transition between no dislodgement and dislodgement by rotation occurs at a flow speed of $u = 5.5ms^{-1}$. The flow speed increases from $5.5ms^{-1}$ to $7.0ms^{-1}$ from $\eta = 2.00m$ to $\eta = 1.00m$. In Fig. 4d, the roughness is 1.4 m and the slope is 10.0^o. In this case, the roughness requires that vertical sliding as described in section 2.2 lifts the boulder up to a position where it can be dislodged. The minimum flow speed for dislodgement is now constant at $7.9ms^{-1}$ for all flow depths.

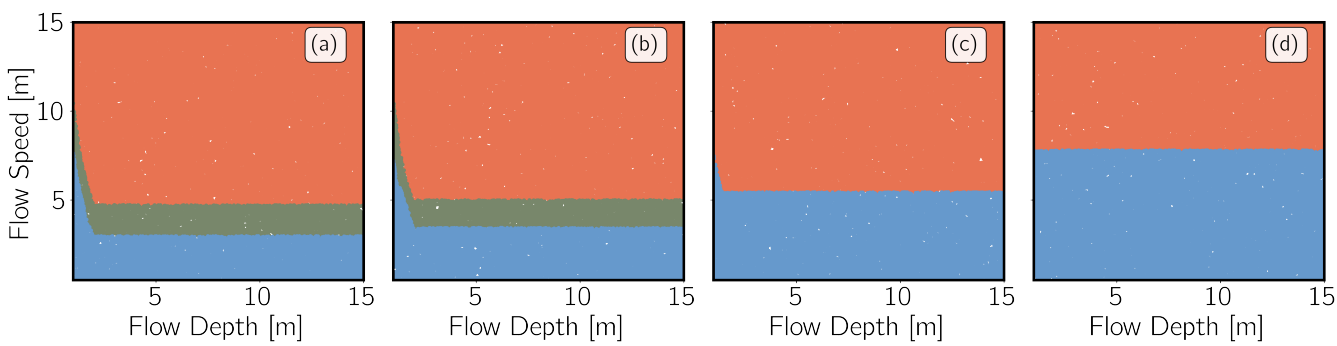

Figure 4: Flow depth - flow speed plot showing no dislodgement (blue), dislodgement by sliding only (green, occurs only when $\delta = 0.0m$) and dislodgement by rotation (orange; includes both rotation and sliding when $\delta = 0.0m$ only) for different roughness values, δ, and slopes, α: (a) $\delta = 0.0m$, $\alpha = 0.0^o$, (b) $\delta = 0.0m$, $\alpha = 10.0^o$, (c) $\delta = 0.8m$, $\alpha = 0.0^o$, and (d) $\delta = 1.4m$, $\alpha = 10.0^o$. Note the boulder dimensions were held constant at $2m \times 2m \times 2m$ with a density of $\rho = 1800kg\,m^{-3}$.

3.3. Dependence on Roughness and Slope Angle

Figure 4a-c indicates the importance of roughness and slope, a topic that was also assessed by Weiss (2012) for spherical boulders. Assuming a Froude number $Fr = 1.0$, Fig. 5 depicts dislodgement as a function of normalized flow depth and roughness in Fig. 5a and normalized flow speed and roughness in Fig. 5b for slope angles from -10° to 10°. For the normalized flow depth as the function of roughness, we see that there is a nonlinear relationship between flow depth and roughness. Furthermore, we can detect that positive slope angles (per definition in Fig. 1, uphill) exhibit a higher-magnitude, but over a much narrower band of

flow depth,s for dislodgement than negative angles (downhill). For positive angles, the narrow flow-depth band becomes even more narrow for larger roughness values. Interestingly, for negative slope values, we find that the flow-depth band widens as the roughness increases.

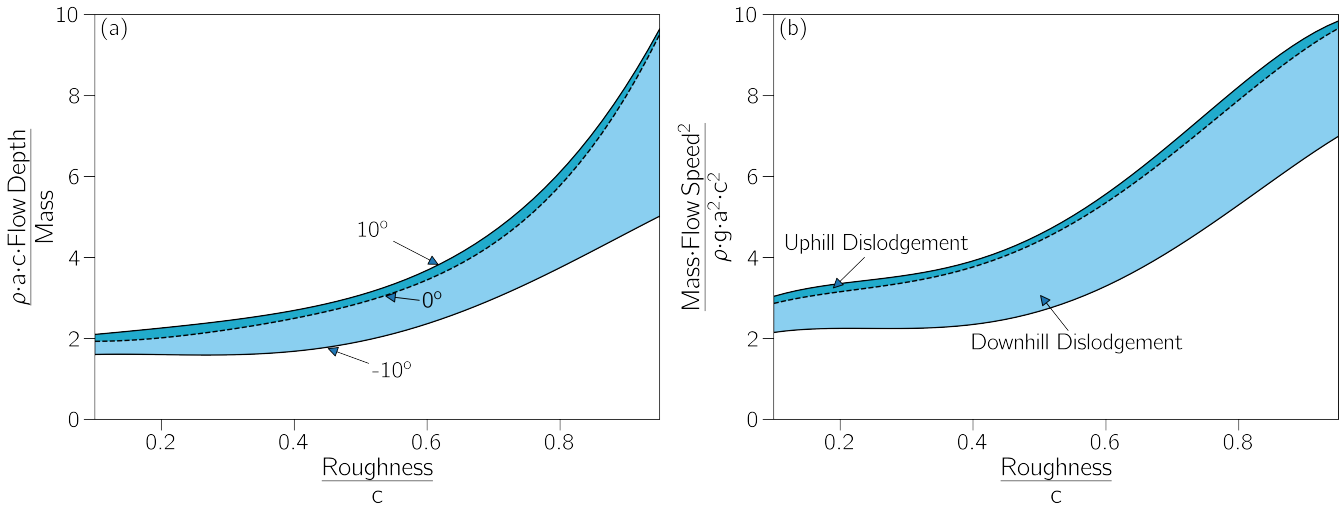

Figure 5: Normalized flow depth (a) and flow speed (b) for dislodgement by rotation as a function of roughness for a range of slopes ($-10^o \geq \alpha \leq 10^o$). A Froude Number of $Fr = 1.0$ is assumed in this analysis

The relationship between the normalized flow speed needed for dislodgement and roughness is likewise nonlinear, while, as in the relationship between flow depth and roughness, the flow-speed band for positive slope angles has a higher magnitude and is much narrower than for negative flow angles. The width of the flow speed band for positive slope angles appears to remain constant; while the flow speed generally increased with increasing roughness (roughness/c-axis of boulder). The increase in flow speed occurs in a linear fashion up to a roughness of 0.74 and then doubles from there onward to a roughness of 1. The flow-speed band for negative slope angles has a similarly complex behavior as its narrowest range occurring at the lowest roughness of 0.17, then the range of the flow speed band increases moderately up to a roughness of 0.74.

4. Discussion and Conclusions

We presented a new model that is based on the conservation of angular momentum for dislodgement by rotation, and an adapted version of Newton's Second Law of Motion for dislodgement by sliding. Recall that dislodgement by sliding is only possible if there is no obstruction, herein roughness ($\delta = 0.0m$), in front of the boulder. The basic idea of using a time-dependent motion of the boulder to a critical point for dislodgement is extended from Weiss and Diplas (2015), especially the rotation part is in comparison to Weiss and Diplas (2015) much more complete by considering partially submerged boulders and by considering rectangular prisms rather than spheres. It should be noted that the model proposed herein can readily be extended to other geometric shapes as well. An important addition to simulating dislodgement by rotation

is the inclusion of vertical sliding so that rotation is possible even if the boulder's center of mass is initially below the pivot point. Namely, the inclusion of vertical sliding enables the flow to lift the boulder upward until its center of mass is at the height of the pivot point, at which time a positive moment is possible. As far as we know, no existing boulder models consider this important process, which is especially important for quarrying boulders from their original stratigraphic units, such as described in Switzer and Burston (2010), and references therein.

Our simulation results presented in Figs. 4 and 5, lead to conclusions about the importance of mass, slope, and roughness in front of the boulder that are similar to those presented in Weiss (2012), Weiss and Diplas (2015), and Weiss and Sheremet (2017). For our presumed boulder shapes, our results indicate that the roughness is a much more sensitive parameter compared to the slope. Fig. 5 reveals a nonlinear influence of roughness on flow speed and flow depth, but also a nonlinear influence of the slope, which is interesting given the simplicity of our approach. While Nott (2003) was the first one to highlight the importance of environmental conditions for boulder dislodgement, Cox et al. (2020) discussed shortcomings in approach that was proposed in Nott (2003).

The exhibited constant flow speed threshold for dislodgement over part of the flow depth interval as shown in Fig. 4, gives rise to the possibility to present the results as a range of possible flow depths for a meaningful flow speed interval or Froude number, in the absence of flow depth markers. However, if flow-depth markers exist, it can help to better characterize hydrodynamic processes also by means of the Froude number, and thereby also be used to check that the ranges of the parameters were chosen to represent the environmental and flow conditions sufficiently well.

Aside from our results, the model that we propose is a significant improvement from previous models in that the possibility to create ensemble and Monte-Carlo-type simulations enables us to include a range of possible transport-related parameters and environmental conditions for boulder transport. Variability of initial conditions or environmental parameters can also be sampled from the distributions, creating Monte-Carlo simulations. This flexibility is important and generates an exploratory model framework that helps us to better understand the sensitive parameters of boulder transport, and if combined with field data a more robust inversion of flow conditions for boulder transport, especially for situations in which environmental parameters, such as slope and roughness in front of the boulder have to be estimated with considerable uncertainty.

References

Barbano, M., Pirrotta, C., Gerardi, F., 2010. Large boulders along the south-eastern Ionian coast of Sicily: Storm or tsunami deposits? Marine Geology 275, 140–154.

Benner, R., Browne, T., Brückner, H., Kelletat, D., Scheffers, A., 2010. Boulder transport by waves: progress in physical modelling. Zeitschrift für Geomorphologie 54, 127–146.

Bourke, P., 1988. Calculating the area and centroid of a polygon. URL: https://www.seas.upenn.edu/~sys502/extra_materials/Polygoni%20Area%20and%20Centroid.pdf. accessed: 13 February 2020.

Buckley, M.L., Wei, Y., Jaffe, B.E., Watt, S., 2012. Inverse modeling of velocities and inferred cause of overwash that emplaced inland fields of boulders at Anegada, British Virgin Islands. Natural Hazards 63, 133–149.

Cox, R., Ardhuin, F., Dias, F., Autret, R., Beisiegel, N., Earlie, C., Herterich, J., Kennedy, A., Paris, R., Raby, A., Schmitt, P., Weiss, R., 2020. Systematic review shows that work done by storm waves can be misinterpreted as tsunami-related, because commonly used hydrodynamic equations are flawed. Frontiers in Marine Science 7. doi:10.3389/fmars.2020.00004.

Cox, R., Zentner, D., Kirchner, B., Cook, M., 2012. Boulder Ridges on the Aran Islands (Ireland): Recent Movements Caused by Storm Waves, Not Tsunamisi. The Journal of Geology 120, 249–272.

Dewey, J., Ryan, P., 2017. Storm, rogue wave, or tsunami origin for megaclast deposits in western Ireland and North Island, New Zealand? Proceedings of the National Academy of Sciences 114, E10639–E10647.

Kennedy, A.B., Mori, N., Zhang, Y., Yasuda, T., Chen, S.E., Tajima, Y.and Pecor, W., Toride, K., 2016. Observations and Modeling of Coastal Boulder Transport and Loading During Super Typhoon Haiyan. Coastal Engineering Journal 58, 1640004. doi:10.1142/S0578563416400040.

Nandasena, N.A.K., Paris, R., Tanaka, N., 2011a. Numerical assessment of boulder transport by the 2004 Indian ocean tsunami in Lhok Nga, West Banda Aceh (Sumatra, Indonesia). Computers & Geosciences 37, 1391–1399.

Nandasena, N.A.K., Paris, R., Tanaka, N., 2011b. Reassessment of hydrodynamic equations to initiate boulder transport by high-energy events (storms, tsunamis). Marine Geology 281, 70–84.

Nott, J., 2003. Waves, coastal boulders and the importance of pre-transport setting. Earth and Planetary Science Letters 210, 269–276.

Switzer, A., Burston, J., 2010. Competing mechanisms for boulder deposition on the southeast Australian coast. Geomorphology 114, 42–54.

Watanabe, M., Goto, K., Imamura, F., Kennedy, A., Sugawara, D., Nakamura, N., Tonosaki, T., 2019. Modeling boulder transport by coastal waves on cliff topography: Case study at hachijo island, japan. Earth Surface Processes and Landforms 44, 2939–2956. doi:10.1002/esp.4684.

Weiss, R., 2012. The mystery of koulders moved by tsunamis and storms. Marine Geology 295-298, 28–33.

Weiss, R., Diplas, P., 2015. Untangling boulder dislodgment in storms and tsunamis: Iis it possible with simple theories? Geophysics, Geochemistry, Geosystems 16, 89–898.

Weiss, R., Sheremet, A., 2017. Toward a new paradigm for boulder dislodgement during storms. Geochemistry, Geophysics, Geosystems 18, 2717–2726. doi:https://doi.org/10.1002/2017GC006926.

Zainali, A., Weiss, R., 2015. Boulder dislodgement and transport by solitary waves: Insights from three-dimensional numerical simulations. Geophysical Research Letters 42, 4490–4497.